The docking protein FRS2α is a critical regulator of VEGF receptors signaling

Pei-Yu Chen[a], Lingfeng Qin[b], Zhen W. Zhuang[a], George Tellides[b], Irit Lax[c], Joseph Schlessinger[c,1], and Michael Simons[a,d,1]

[a]Yale Cardiovascular Research Center, Department of Internal Medicine, and Departments of [b]Surgery, [c]Pharmacology, and [d]Cell Biology, Yale University School of Medicine, New Haven, CT 06520

Contributed by Joseph Schlessinger, March 11, 2014 (sent for review January 28, 2014)

Vascular endothelial growth factors (VEGFs) signal via their cognate receptor tyrosine kinases designated VEGFR1-3. We report that the docking protein fibroblast growth factor receptor substrate 2 (FRS2α) plays a critical role in cell signaling via these receptors. In vitro FRS2α regulates VEGF-A and VEGF-C–dependent activation of extracellular signal-regulated receptor kinase signaling and blood and lymphatic endothelial cells migration and proliferation. In vivo endothelial-specific deletion of FRS2α results in the profound impairment of postnatal vascular development and adult angiogenesis, lymphangiogenesis, and arteriogenesis. We conclude that FRS2α is a previously unidentified component of VEGF receptors signaling.

phosphorylation | MAP kinase | FGF receptor | signal transduction | receptor kinase inhibition

Vascular endothelial growth factors (VEGFs) are key regulators of blood and lymphatic vessel development and homeostasis. The absence of VEGF-A during development results in a complete failure of blood vasculature formation (1), whereas VEGF-C knockout abolishes lymphangiogenesis (2). Both VEGF-A and VEGF-C play equally critical roles in postnatal formation and maintenance of various blood and lymphatic vessel beds (3–6). The two VEGFs signal via, respectively, the two receptor tyrosine kinases (RTK) VEGFR2 and VEGFR3 with the former primarily expressed in the arterial and venous vasculature and the latter in the lymphatic vasculature in adult tissues (7). The other VEGF receptor, VEGFR1, is thought to function largely as a "decoy" receptor in endothelial cells but can transmit signaling in mononuclear cells (7).

All VEGF receptors share a number of structural similarities including an extracellular ligand binding domain, a single transmembrane region, and a cytoplasmic domain containing a tyrosine kinase domain with an insert region. Receptor activation requires ligand-induced dimerization that results in autophosphorylation of cytoplasmic tyrosines that serve as binding sites for various signaling proteins. In the case of VEGF-A receptor, VEGFR2 phosphorylation of Y^{1054}/Y^{1059} is required for maximal VEGFR2 kinase activity that leads to phosphorylation of Y^{1175} (a phospholipase Cγ1 binding site also required for ERK activation) and Y^{951} (a TSAd binding site leading to Src activation) among others (7). VEGF-C signals via VEGFR3 in a similar manner.

In the course of studying fibroblast growth factor (FGF) signaling, we noticed that an endothelial knockdown or deletion of a scaffold protein FRS2α, known to be involved in FGF and neural growth factor (NGF) receptor signaling (8–10), also affects VEGF signaling. FRS2α is a docking protein that contains an N-terminal myristylation site, a PTB domain, and a large C-terminal tail that contains four binding sites for the SH2 domain of the adaptor protein Grb2 and two binding sites for the SH2 domain of the tyrosine phosphatase Shp2 (11). Tyrosine phosphorylation of FRS2α at these binding sites leads to activation of MAPK signaling (12).

In this study, we found that FRS2α plays a central role in regulation of VEGF signaling in blood and lymphatic endothelial cells. Its deletion profoundly reduced VEGF signaling in vitro and in vivo and resulted in impairment of postnatal vascular development and adult angiogenesis, lymphangiogenesis, and arteriogenesis.

Results

A knockdown of FRS2α expression in HUVEC resulted in a profound decrease in VEGFR2 phosphorylation following VEGF-A_{165} treatment as demonstrated by immunoblotting of ligand-stimulated cell lysates with phosphotyrosine-specific antibodies or with phosphorylation site-specific antibodies (Fig. 1 *A* and *B*). These results were confirmed in studies by using expression of a dominant-negative FRS2α mutant $FRS2α^{6F}$ that has all six tyrosines normally phosphorylated by FGF receptors replaced with phenylalanines (13) (Fig. 1*C*). In addition, reducing FRS2α expression or $FRS2α^{6F}$ overexpression profoundly inhibited VEGF-A_{165}–induced ERK signaling (Fig. 1 *B* and *C*). The observed inhibition of VEGF signaling following FRS2α knockdown resulted in profound reduction of VEGF-driven HUVEC proliferation, migration, and matrigel cords formation (Fig. 1 *D* and *E*).

Whereas VEGFR2 is the major VEGF receptor in blood endothelial cells, VEGFR3 is the major receptor in the lymphatic endothelium. A knockdown of FRS2α in human dermal lymphatic endothelial cells (HDLEC) resulted in a significant reduction of VEGFR3 activation in response to VEGF-C treatment (Fig. 2*A*) and a reduction in VEGF-C–induced ERK1/2 activation (Fig. 2*B, Upper*). Expression of a dominant-negative FRS2α mutant $FRS2α^{6F}$ in HDLEC showed a similar effect (Fig. 2*B, Lower*).

As in the case of HUVEC, this phenomenon translated in reduced proliferation and migration of HDLEC in response to VEGF-C (Fig. 2*C*). Finally, VEGFR1 activation by PlGF in HUVEC was also inhibited by FRS2α knockdown (Fig. 2*D*). The decreased signaling response to VEGF-A was independent of the isoform used. Stimulation of HUVEC with VEGF-A_{121} that signals via VEGFR2 but, unlike VEGF-A_{165}, does not require binding to neuropilin-1, resulted in similarly decreased VEGFR2

Significance

Regulation of vascular endothelial growth factor (VEGF) signaling plays a central role in a range of biological processes from embryonic and perinatal vascular development to maintenance of the mature adult vasculature to regulation of various organs function. We report that the intracellular docking protein FRS2α, not hitherto known to be involved in VEGF signaling, plays a critical role in regulation of this process.

Author contributions: P.-Y.C., L.Q., Z.W.Z., G.T., I.L., J.S., and M.S. designed research; P.-Y.C., L.Q., Z.W.Z., and G.T. performed research; P.-Y.C., L.Q., Z.W.Z., I.L., J.S., and M.S. analyzed data; and P.-Y.C., L.Q., Z.W.Z., I.L., J.S., and M.S. wrote the paper.

The authors declare no conflict of interest.

[1]To whom correspondence may be addressed. E-mail: michael.simons@yale.edu or joseph.schlessinger@yale.edu.

This article contains supporting information online at www.pnas.org/lookup/suppl/doi:10.1073/pnas.1404545111/-/DCSupplemental.

www.pnas.org/cgi/doi/10.1073/pnas.1404545111

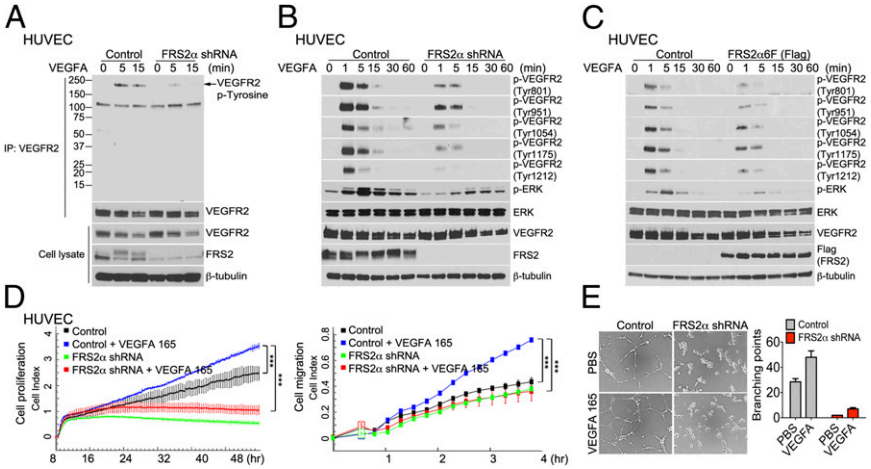

Fig. 1. FRS2α knockdown in HUVEC inhibits VEGF-A_{165}–dependent signaling. (*A*) Control and FRS2α knockdown HUVEC were serum starved overnight and treated with VEGF-A_{165} (50 ng/mL) as indicated. Cell lysates were immunoprecipitated (IP) with an anti-VEGFR2 antibody and immunoblotted with anti–p-Tyrosine antibody. The same blot was stripped and blotted with anti-VEGFR2. Input lysates were blotted with anti-VEGFR2 and anti-FRS2α antibodies. (*B*) Control and FRS2α knockdown HUVEC were serum starved overnight and treated with VEGF-A_{165} (50 ng/mL) as indicated. Cell lysates were blotted with p-VEGFR2, VEGFR2, p-ERK, ERK, and FRS2α antibodies. (*C*) Control and FRS2α-6F (Flag) overexpressed HUVEC were serum starved overnight and treated with VEGF-A_{165} (50 ng/mL). Cell lysates were blotted with p-VEGFR2, VEGFR2, p-ERK, ERK, and Flag (FRS2α) antibodies. (*D*) Control and FRS2α knockdown HUVEC were serum starved overnight. Cell proliferation (*Left*) and cell migration (*Right*) in response to VEGF-A_{165} (50 ng/mL) profiles are shown as detected by xCELLigence. Approximately 1000 cells (for cell proliferation) or 25,000 cells (for cell migration) were loaded per well in duplicate (***$P < 0.01$ compared with control). (*E*) In vitro Matrigel: The extent of cords branching was assessed in control and FRS2α knockdown HUVEC placed on growth factor-depleted Matrigel and exposed to VEGF-A_{165} (50 ng/mL). Data in *A*–*C* and *E* are based three independent experiments; data in *D* are based on two independent experiments.

activation (Fig. S1*A*) as was the response to VEGF-C (Fig. S1*B*). To demonstrate that this response to VEGF following FRS2α knockdown is specific to receptors interacting with FRS2α, HUVEC and HDLEC were treated with EGF. The experiment presented in Fig. S1 *C* and *D* showed that FRS2α knockdown had no effect on EGF-induced ERK activation.

Because the VEGF-ERK pathway plays an important role in postnatal vascular development and adult angiogenesis and arteriogenesis, we next investigated whether any vascular abnormalities are present in *Frs2*α mutant mice. As previously reported, homozygous *Frs2*α*4F* mutants ($Frs2\alpha^{4F/4F}$, deficient in Grb-2 binding) are viable (14), whereas homozygous $Frs2\alpha^{2F/2F}$ mutants (deficient in Shp-2 binding) exhibit a profound decrease in ERK activity and die during embryonic development (15). Because it is difficult to distinguish whether developmental defects in $Frs2\alpha^{2F/2F}$ mutants are due to abnormalities of VEGF or FGF signaling, we concentrated on adult $Frs2\alpha^{4F/4F}$ mice.

$Frs2\alpha^{4F/4F}$ knock-in mice are born at the appropriate Mendelian frequency but are significantly smaller than their wild-type littermates (Fig. S2 *A* and *B*). Examination of heart, lung, and liver vasculature demonstrated comparably normal vascular architecture, and expression levels of VE-cadherin and VEGFR2 mRNAs were similar to wild-type mice (Fig. S2*C*), thereby suggesting comparable endothelial cell mass and normal developmental angiogenesis.

VEGF-A is an important driver of arteriogenesis (16). To examine the effect of this mutation on arteriogenesis, we used a hindlimb ischemia femoral artery ligation model. Laser-Doppler analysis of the distal limb blood flow, expressed as a ratio of flow in the ischemic to normal limb, demonstrated a significantly impaired recovery in $Frs2\alpha^{4F/4F}$ mutants (Fig. S3 *A* and *B*). In addition, mutant mice demonstrated more severe tissue damage as judged by clinical scores (Fig. S3*C*). Because growth of new arterial vasculature is the principal mechanism leading to the restoration of distal blood flow in this model, we next performed micro-computed tomography (micro-CT) analysis of the arterial hindlimb vasculature 14 d after the initial surgery. In agreement with the finding of impaired distal blood flow recovery, micro-CT demonstrated decreased arteriogenesis in $Frs2\alpha^{4F/4F}$ mice compared with top controls (Fig. S3 *D* and *E*). Thus, $Frs2\alpha^{4F/4F}$ mutation is associated with normal vascular development but reduced adult angiogenesis and arteriogenesis.

To test whether vascular responses to VEGF are also affected, we used in vivo Matrigel and ear angiogenesis models. Implantation of Matrigel plugs with VEGF-A_{165} or injection of VEGF-A_{164} adenovirus led to extensive angiogenesis in control animals, whereas the response to VEGF-A was significantly reduced in $Frs2\alpha^{4F/4F}$ mutants (Fig. S3 *F* and *G*). To confirm the relevance of our findings in $Frs2\alpha^{4F/4F}$ knock-in animals, we generated mice with endothelial-specific inducible deletion of *Frs2*α (use $Frs2\alpha^{-/-}$ *to* describe endothelial cell-specific knockout) by using Cdh5-CreERT2 and PDGF-BB-CreERT2 mouse lines.

We first studied adult angiogenesis. Injection of the Ad-VEGF-A_{164} virus into mouse ear pads induces intense local angiogenesis. This response was significantly reduced in $Frs2\alpha^{-/-}$ mice compared with control littermates (Fig. 3 *A* and *B*). Implantation of VEGF-A_{165} impregnated Matrigel pellets into $Frs2\alpha^{-/-}$ also resulted in a significantly reduced angiogenic response compared with implantations in littermate controls (Fig. 3 *C* and *D*). Finally, similar results were obtained with VEGF-A_{164} and VEGF-C corneal implants (Fig. 3 *E*–*H*).

To test the effect of endothelial *Frs2*α deletion on arteriogenesis, we used a hindlimb ischemia model. Ligation of the right common femoral artery leads to nearly 90% reduction in the blood flow to the ipsilateral paw as demonstrated by laser-Doppler flow imaging (Fig. 4 *A* and *B*). Although control mice recovered blood flow 14 d later, $Frs2\alpha^{-/-}$ demonstrated a significantly reduced flow restoration and a significantly increased loss of tissues in the ischemic foot (Fig. 4 *A*–*C*). In addition, examination of capillary growth in the ischemic part of the foot demonstrated reduced angiogenesis in $Frs2\alpha^{-/-}$ mice (Fig. 4 *D* and *E*).

VEGF-A signaling plays a critical role in postnatal development of retinal vasculature. To examine the role of *Frs2*α in this process, Cdh5-CreERT2 or PDGF-BB-CreERT2 was activated at postnatal day 1 (P1). When examined 5 d later at P6, $Frs2\alpha^{-/-}$ mice demonstrated a profound reduction in the retinal

BIOCHEMISTRY

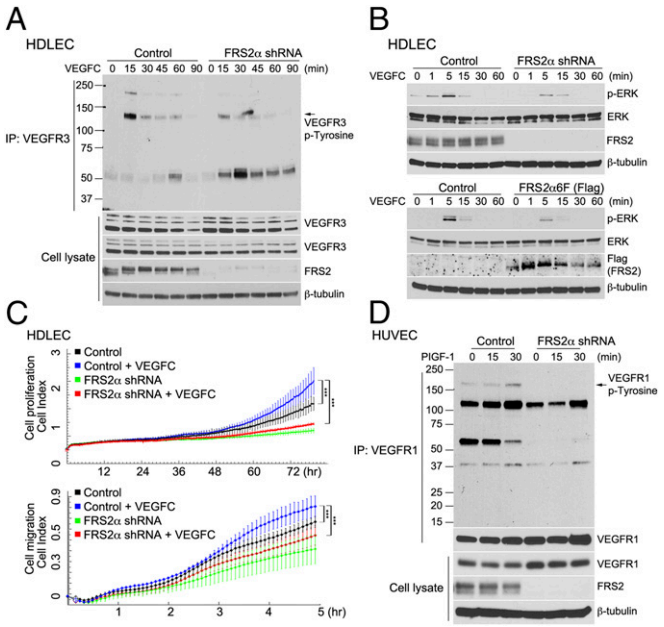

Fig. 2. FRS2α knockdown in HDLEC inhibits VEGF-C–dependent signaling. (*A*) Control and FRS2α knockdown HDLEC were serum starved overnight and treated with VEGF-C (50 ng/mL) for the indicated times. Cell lysates were immunoprecipitated (IP) with an anti-VEGFR3 antibody and immunoblotted with anti–p-Tyrosine antibody. The same blot was stripped and blotted with anti-VEGFR3. Input lysates were blotted with anti-VEGFR3 and anti-FRS2α antibodies. (*B Upper*) Control and FRS2α knockdown HDLEC were serum starved overnight and treated with VEGF-C (50 ng/mL). Cell lysates were blotted with p-ERK, ERK, and FRS2α antibodies. (*B Lower*) Control and FRS2α6F (Flag) overexpressed HDLEC were serum starved overnight and treated with VEGF-C (50 ng/mL). Cell lysates were blotted with p-ERK, ERK, and FRS2α antibodies. (*C*) Control and FRS2α knockdown HDLEC were serum starved overnight. Cell proliferation (*Upper*) and cell migration (*Lower*) in response to VEGF-C (50 ng/mL) profiles, detected by xCELLigence. Approximately 1,000 cells (for cell proliferation) or 25,000 cells (for cell migration) were loaded per well in duplicate (***$P < 0.01$ compared with control). (*D*) Control and FRS2α knockdown HUVEC were serum starved overnight and treated with PlGF-1 (50 ng/mL). Cell lysates were immunoprecipitated (IP) with an anti-VEGFR1 antibody and immunoblotted with anti–p-Tyrosine antibody. The same blot was stripped and blotted with anti-VEGFR1. Input lysates were blotted with anti-VEGFR1 and anti-FRS2α antibodies. Data shown in *A*, *B*, and *D* are based on three independent experiments; data in *C* are based on two independent experiments.

vascular coverage (Fig. 5 *A–D*) In addition to retina vasculature abnormalities, *Frs2*$\alpha^{-/-}$ mice showed a ∼50% reduction in the number of diaphragm lymphatic vessels (Fig. 5 *E* and *F*). Together these results demonstrate the critical role played by FRS2α in mediation of VEGF signaling in vivo.

Discussion

The findings in this study identify FRS2α as a unique regulator and important intracellular signaling via VEGFRs. As demonstrated in the case of VEGFR2 and VEGFR3, the absence of FRS2α leads to impaired activation of VEGF-A– and VEGF-C–induced signaling in, respectively, blood and lymphatic endothelial cells. In vivo this phenotype translates to profound impairment of angiogenesis and arteriogenesis (VEGF-A–dependent processes) and lymphangiogenesis (VEGF-C–dependent process).

FRS2α involvement in VEGF signaling is highly unexpected because VEGFR2 lacks obvious canonical FRS2α binding sites. Numerous proteins have been proposed to function downstream of VEGFR2 transmitting its intracellular signals including TSAd, PLCγ, and Grb2 among others (7). T-cell–specific adapter molecule (TSAd) binds to the VEGFR2 Y^{951} site. TSAd is critical for actin reorganization in cell culture models and activation of Src but is not essential for mouse development (17, 18). Grb2 binds to the VEGFR2 Y^{1212} site, but its role is uncertain because mouse VEGFR2 Y^{1212} mutants have no discernible defects (19). PLCγ binds to the Y^{1175} site and activates MAPK signaling. Mice carrying a VEGFR2 Y1175F mutation die between embryonic day (E) 8.5 and E9.5 with endothelial and hematopoietic defects, similar to those seen in *Vegfr2*$^{-/-}$ mice (19). Given these considerations, it will be important to determine the precise mechanism of FRS2α-dependent regulation of VEGF signaling.

Such a critical involvement of FRS2α in VEGF signaling points to a new role for this molecule. To date, FRS2α has been implicated in biological activities regulated by FGF and NGF including cell proliferation and migration, outgrowth of neuritis, and development of various organs and tissues (11, 20). *Frs2*$\alpha^{-/-}$ mice die at E7.0–E7.5 because of multiple developmental problems including abnormal anterior-posterior axis formation, failure of development of the extraembryonic ectoderm, cerebral cortex, eye, carotid body, cardiac outflow tract, prostate, limbs and skeleton, and widespread vascular abnormalities (21).

The current study provides the first evidence that vascular defects seen in these mice may be due to the impairment of VEGF signaling. *Frs2*$\alpha^{2F/2F}$ knock-in mice die during embryonic development with embryos showing profound growth retardation and extensive edema. As we demonstrate in this study, *Frs2*$\alpha^{4F/4F}$ knock-in mice also reveal a number of angiogenic and arteriogenic defects including decreased responsiveness to VEGF stimulation in vivo. However, because it is difficult to conclusively tease out VEGF-dependent abnormalities in mice lines with global disruption of FRS2α expression, we studied vascular defects in mice with endothelial-specific deletion of *Frs2*α initiated after birth.

Injection of Ad-VEGF-A in the ear of these mice or insertion of a VEGF-A–containing Matrigel plug led to a markedly muted angiogenic response than seen in littermate controls. Similarly, the early postnatal development of the retina vasculature, a process that is largely VEGF driven, was also dramatically impaired in *Frs2*$\alpha^{-/-}$ mice. Finally, a study of arteriogenesis using a hindlimb ischemia model also demonstrated a profound retardation of arterial network formation that is comparable to that seen in other genetic mice models with impaired VEGF-dependent activation of MAPK signaling (16, 22). Taken together, these data point to a critical role played by endothelial FRS2α in vascular development, angiogenesis, lymphangiogenesis, and arteriogenesis. The precise mechanism responsible for FRS2α-dependent regulation of VEGF receptor signaling remains uncertain and is the subject of ongoing studies. It should be noted that although FRS2α phosphorylation by VEGF in EC has been reported (23), no functional significance of this event has been suggested and FRS2α involvement in VEGF signaling is not typically considered (7).

In the vascular system, VEGF and FGF play central, if somewhat different, roles in the regulation of vascular development and maintenance of vascular homeostasis. The unexpected role of FRS2α in VEGFR signaling has profound biological implications because the fact that a single molecule affects both VEGF and FGF signaling pathways is critically important, not only for our understanding of VEGF biology per se, but also for understanding of VEGF/FGF (or, potentially other RTK) cross-talk and the development of drugs designed to selectively (or jointly) affect VEGF and FGF signaling. The latter, in turn, is crucial to the development of therapeutic interventions aimed at both stimulation and inhibition of blood vessel growth.

In summary, in this study we showed that FRS2α binds to and regulates signaling of all three VEGF receptors. This result places this molecule at the center of VEGF and endothelial cell biology.

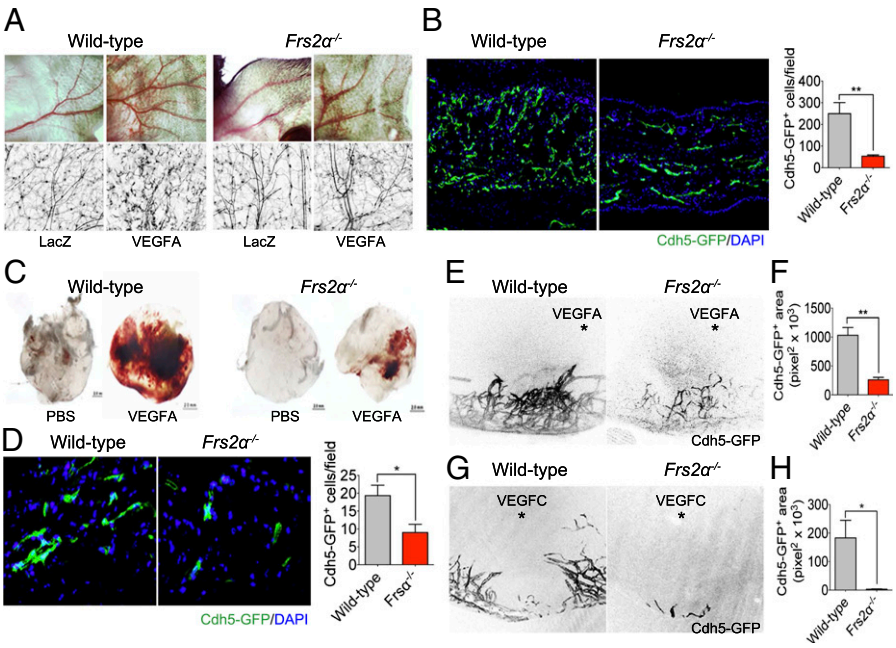

Fig. 3. Impaired angiogenesis in $Frs2\alpha^{-/-}$ mice. (*A*) Wild-type and $Frs2\alpha^{-/-}$ mice were treated with 1×10^9 pfu of Ad-LacZ or Ad-VEGF-A_{164} virus. VEGF-A–induced angiogenesis was recorded at day 7 by using a stereomicroscope and fluorescent scope. (*B*) Mouse ears were sectioned, and the number of vessels was counted (**$P < 0.01$ compared with control) ($n = 4$ mice per group). (*C* and *D*) Matrigel mixed with either PBS or VEGF-A_{165} (50 ng/mL) were placed s.c. in wild-type or $Frs2\alpha^{-/-}$ mice. On day 7, matrigel plugs were sectioned, and the number of vessels was counted (*$P < 0.05$ compared with control) ($n = 6$ mice per group). (*E–H*) Hydron pellet containing VEGF-A_{164} or VEGF-C was implanted into the cornea of wild-type and $Frs2\alpha^{-/-}$ mice. Angiogenesis was assessed by stereo microscopy at day 7 following implantation (*E* and *G*) (asterisk marks the position of the implanted pellet). Vascular density was quantified in *F* and *H* (*$P < 0.05$; **$P < 0.01$ compared with control) ($n = 6$ mice per group).

Materials and Methods

Growth Factors. All recombinant human growth factors including EGF (Sigma E9644; for in vitro stimulation), VEGF-A_{165} (R&D Systems 293-VE-010; for in vitro stimulation), VEGF-A_{121} (R&D Systems 4644-VS-010; for in vitro stimulation), VEGF-C (R&D Systems 2179-VC-025; for in vitro stimulation), VEGF-C (R&D Systems 2179-VC-025/CF; for in vivo corneal angiogenesis assay), PlGF-1 (Peprotech 100–06; for in vitro stimulation), and recombinant mouse VEGF-A_{164} (R&D Systems 493-MV-005/CF; for in vivo corneal angiogenesis assay) were reconstituted in 0.1% BSA/PBS.

Generation of Lentiviruses. FRS2α shRNA lentiviral constructs were purchased from Open Biosystem. The generation and production of FRS2α lentivirus was described (24). For the production of FRS2α6F, 10 μg of pLVX-IRES-puro carrying the $Frs2\alpha^{6F}$ cDNA expression cassette, 5 μg of pMDLg/PRRE, 2.5 μg of RSV-REV, and 3 μg of pMD.2G were cotransfected into 293T cells by using FuGENE 6. Forty-eight hours later, the medium was harvested, cleared by 0.45-μm filter, mixed with polybrene (Sigma), and applied to cells. After 6 h of incubation, the virus-containing medium was replaced with fresh medium.

Antibodies Used for Immunodetection of Proteins The following antibodies were used for immunoblotting (IB), immunoprecipitation (IP), or immunohistochemistry (IHC): CD31 (ab28364, Abcam; IHC), CD31 (553370, BD Pharmingen; EC isolation), p-ERK (M8159, Sigma; IB), FLAG (F1804, Sigma; IB),

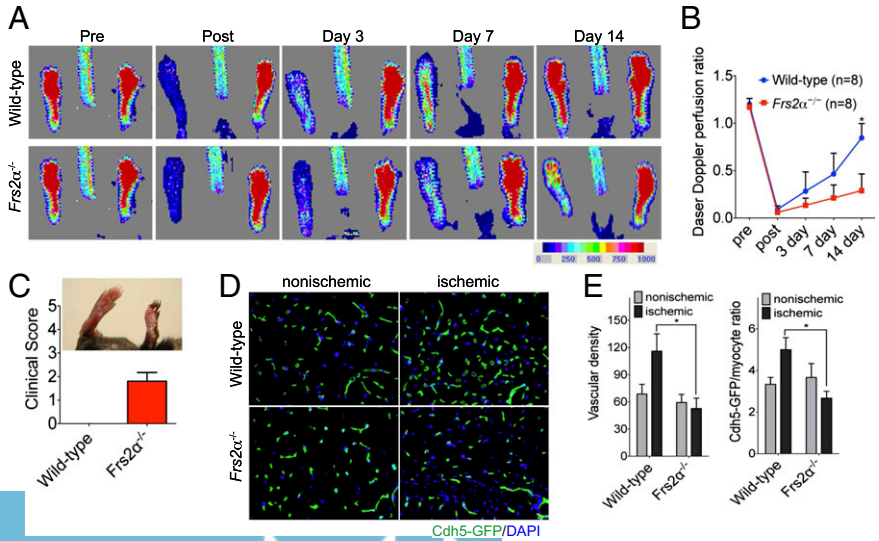

Fig. 4. Impaired arteriogenesis in $Frs2\alpha^{-/-}$ mice. (*A*) Laser Doppler images showing blood flow before and after the induction of ischemia to the left hindlimb in wild-type and $Frs2\alpha^{-/-}$ mice. (*B*) Laser-Doppler analysis of blood flow recovery in the left foot, expressed as a ratio of blood flow in left to right foot (L/R). *$P < 0.05$, wild-type vs. $Frs2\alpha^{-/-}$ ($n = 8$ mice per group). (*C*) In $Frs2\alpha^{-/-}$ mice, clinical score indicated a severe phenotype, leading to necrosis of limb. (*D*) Representative sections from nonischemic and ischemic groups of wild-type and $Frs2\alpha^{-/-}$ on day 14 after ischemia. Quantification of capillary density (number/mm^2 muscle area) and ratio of CD31/myocyte are shown in *E*. Data are mean ± SD from 10 fields per section (3 sections per mouse; $n = 4$ for each strain). *$P < 0.05$, wild-type vs. $Frs2\alpha^{-/-}$.

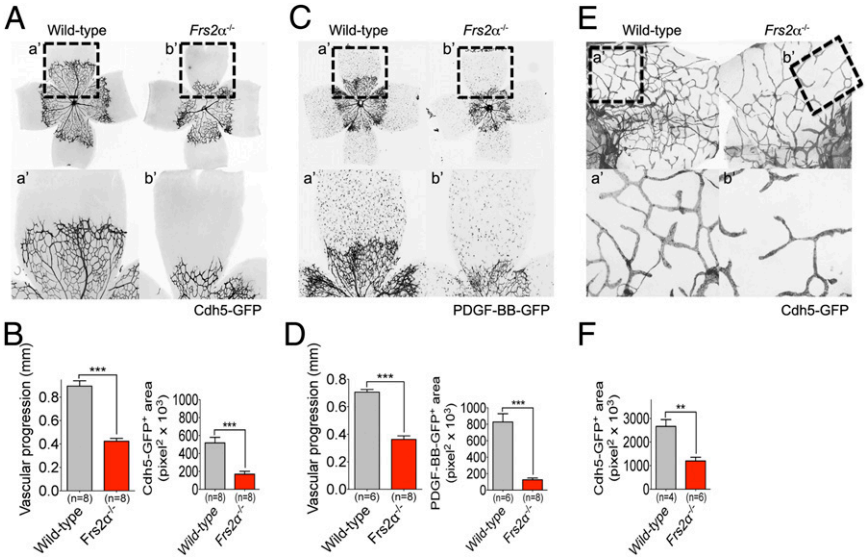

Fig. 5. Postnatal angiogenesis and lymphangiogenesis defects in *Frs2*$\alpha^{-/-}$ mice. (*A–D*) P6 retinas from wild-type and *Frs2*$\alpha^{-/-}$ littermate mice. (*E* and *F*) P6 diaphragms from wild-type and *Frs2*$\alpha^{-/-}$ littermate mice. *a'* and *b'* panels show higher magnification of the angiogenic front (*A–D*) and diaphragm lymphatic vessels (*E* and *F*).

FRS2α (H-91, Santa Cruz; IB), p44/p42 MAP Kinase (9102, Cell Signaling; IB), Phosphotyrosine, clone 4G10 (05–321, Millipore; IB), Phosphotyrosine (PY20) (sc-508, Santa Cruz; IB), β-tubulin (T7816, Sigma; IB), VEGFR2 (2479, Cell Signaling; IB), VEGFR2 (5168, Cell Signaling; IP), p-VEGFR2 Tyr-801 (VP2921, ECM Biosciences; IB), p-VEGFR2 Tyr-951 (4991, Cell Signaling; IB), p-VEGFR2 Tyr-1054/1059 (441047G, Invitrogen; IB), p-VEGFR2 Tyr-1175 (2478, Cell Signaling; IB), and p-VEGFR2 Tyr-1214 (44-1052, Invitrogen; IB).

Cell Culture and Reagents. ***Cell lines and culture condition.*** Primary human endothelial cell culture: HUVEC (human umbilical vein endothelial cells, passage 5–10; Lonza) and HDLEC (human dermal lymphatic endothelial cells, passage 5–10; Lonza) were cultured in EBM-2 supplemented with EGM-2-MV bullet kit (Lonza). Culture vessels were coated with 0.1% gelatin (G6144; Sigma) for 30 min at 37 °C immediately before cell seeding. For different growth factor treatment, cells were serum starved overnight and treated with 50 ng/mL EGF, VEGF-A_{165}, VEGF-A_{121}, VEGF-C, or PlGF for different time points.
Primary mouse endothelial cell isolation. Primary mouse endothelial cells were isolated from the heart, lung, and liver by using rat anti-mouse CD31 antibody (clone MEC13.3, Pharmingen; 553370) and Dynabeads (catalog no. 110.35; Invitrogen) as described (25).

Cell Lysis, Immunoprecipitation, and Western Blot Analysis. To obtain cell lysates, the cells were washed with cold PBS and lysed for 10 min on ice in a hypotonic HNTG lysis buffer (20 mM Hepes at pH 7.4, 150 mM NaCl, 10% (vol/vol) glycerol, 1% Triton X-100, 1.5 mM $MgCl_2$, 1.0 mM EGTA) containing protease inhibitor mixture (11-697-498-001; Roche), and phosphatase inhibitor mixture (04-906-837-001; Roche). The lysates were centrifuged at 15,871 × *g* at 4 °C for 15 min. The immunoprecipitation and Western blot analysis procedure were described (25).

Matrigel Cord Formation Assay. Twenty-four–well plates were coated with growth factor-reduced Matrigel (354230; BD Biosciences) and allowed to solidify for 30 min at 37 °C. Cells were trypsinized, seeded on Matrigel-coated plates at a density of 6 × 10^4 cells per well in EBM-2 medium with 0.5% FBS with and without VEGF-A, and incubated for 6 h at 37 °C. Photomicrographs were taken at 100× magnification.

xCELLigence Real-Time Cell Analysis: Cell Proliferation and Cell Migration. Cell proliferation and cell migration experiments were carried out by using the xCELLigence Real-Time Cell Analysis (RTCA) DP instrument (Roche Diagnostics) in a humidified incubator at 37 °C and 5% (vol/vol) CO_2.

Cell proliferation experiments were performed by using modified 16-well plates (E-plate; Roche Diagnostics). Initially, 100 μL of cell-free growth medium [20% (vol/vol) FBS] was added to the wells. After leaving the devices at room temperature for 30 min, the background impedance for each well was measured. One hundred microliters of the cell suspension with or without growth factor was then seeded into the wells (1,000 cells per well). Plates were locked in the RTCA DP device in the incubator and the impedance value of each well was automatically monitored by the xCELLigence system and expressed as a cell index value (CI). CI was monitored every 15 min for 300 times. Two replicates of each cell concentration were used in each test. Water was added to the space surrounding the wells of the E-plate to avoid interference from evaporation.

Cell migration experiments were performed by using modified 16-well plates (CIM-16; Roche Diagnostics) with each well consisting of an upper and a lower chamber separated by a microporous membrane containing randomly distributed 8-μm pores.

Initially, 160 μL and 30 μL of media was added to the lower and upper chambers, respectively, and the CIM-16 plate was locked in the RTCA DP device at 37 °C and 5% (vol/vol) CO_2 during 60 min to obtain equilibrium according to the manufacturer's guidelines. After this incubation period, a measurement step was performed as a background signal, generated by cell-free media. To initiate an experiment, 100 μL of the cell suspension was then seeded into the wells (10,000 cells per well). After cell addition, CIM-16 plates were incubated during 30 min at room temperature in the laminar flow hood to allow the cells to settle onto the membrane according to the manufacturer's guidelines.

To prevent interference from evaporation during the experiments, medium was added to the entire empty space surrounding the wells on the CIM-16 plates. Each condition was performed in duplicate with a programmed signal detection schedule of each 5 or 15 min during 5 h of incubation. All data have been recorded by the supplied RTCA software (vs. 1.2.1).

RNA Isolation, Quantitative Real-Time PCR, and Gene Expression Profiling. RNA was isolated using RNeasy plus Mini Kit (74134, Qiagen) and converted to cDNA using iScript cDNA synthesis kit (170-8891, Bio-Rad). Quantitative real-time PCR was performed using Bio-Rad CFX94 by mixing equal amount of cDNAs, iQ SYBR Green Supermix (170-8882; Bio-Rad), and gene specific primers (QIAGEN). All reactions were done in a 25-μL reaction volume in duplicate. Data were normalized to an endogenous control β-actin. Values are expressed as fold change in comparison with control.

Generation of Mice. The *Frs2*$\alpha^{4F/4F}$ mice (26) were provided by V. P. Eswarakumar, Yale University, New Haven, CT. *Frs2*$\alpha^{flox/flox}$ mice were described (27). Cdh5-CreERT2 (28) (gift from R. H. Adams, Max Planck Institute, Munster, Germany) and PDGF-BB-CreERT2 (29) (gift from M. Fruttiger, University College London, London) transgenic mice were first bred with mT/mG [B6,129(Cg)-Gt(ROSA)26Sor$^{tm4(ACTB-tdTomato,-EGFP)Luo}$/J] (JAX SN:007676) mice to generate endothelial cell-specific reporter mice then crossed with *Frs2*$\alpha^{flox/flox}$ mice. To induce Cre recombination for adult angiogenesis and arteriogenesis assay, P6 pups were pipette fed with 0.05 mg/g tamoxifen solution (20 mg/mL

stock solution in corn oil) every other day 10 times. To induce Cre recombination for P6 retina vasculature and diaphragm, P1 pups were pipette fed with 0.05 mg/g tamoxifen solution (20 mg/mL stock solution in corn oil) for five consecutive days. Cross-breeding of these lines with the mT/mG reporter line was used to assess the effectiveness of Cre-driven recombination. For PCR genotyping analysis, the primers used were as follows:

Frs2α4F (5′-AGAATGGTGGCACAAACCAATAATCC-3′ and 5′-CAATTCTTAACACCCACAAGGCCG-3′), *Frs2α*$^{flox/flox}$ (5′-GAGTGTGCTGTGATTGGAAGGCAG-3′ and 5′-GGCACGAGTGTCTGCAGACACATG-3′), mT/mG (5′-CTCTGCTGCCTCCTGGCTTCT-3′, 5′-CGAGGCGGATCACAAGCAATA-3′, and 5′-TCAATGGGCGGGGGTCGTT-3′), Cdh5-CreERT2 (5′-GCCTGCATTACCGGTCGATGCAACGA-3′, and 5′-GTGGCAGATGGCGCGGCAACACCATT-3′), and PDGF-BB-CreERT2 (5′-CCAGCCGCCGTCGCAACTC-3′, and 5′-GCCGCCGGGATCACTCTC G-3′)

Animal Models for Examination of Arteriogenesis and Angiogenesis. All experiments were performed under protocols approved by Yale University Institutional Animal Care and Use Committees.

Mouse ear angiogenesis assay. Adenovirus-encoding VEGF-A_{164} (1×10^9 pfu) or LacZ control virus (1×10^9 pfu) was intradermally injected into mice ear skin.

In vivo matrigel plug assay. Growth factor reduced Matrigel (354230; BD Biosciences) were premixed with VEGF-A_{165} (PHC9391, Invitrogen) and heparin (20 U/mL). The samples were injected into the s.c. tissues of 10-wk-old mice. Once the mice were killed, the recovered Matrigel plugs were fixed in 10% (vol/vol) formalin.

Mouse corneal micropocket assay. Micropellets containing VEGF-A_{164} (493-MV-005/CF; R&D), or VEGF-C (2179-VC-025/CF; R&D) together with the slow-release polymer (sucralfate and hydron polymer) were implanted into micropockets of mouse corneas ($n = 8$ per group). At day 7 after implantation, corneal neovascularization was examined and photographed.

Hindlimb ischemia model and laser Doppler blood flow analysis. Mouse hindlimb ischemia was induced as described (16). For the laser Doppler blood flow analysis, hind limb blood flow was measured on preoperative day and postoperative days 0, 3, 7, and 14 by using a laser Doppler blood flow analyzer (Moor LDI; Moor Instruments). Blood flow was quantitatively assessed as changes in the laser images by using different color pixels. To avoid mouse-to-mouse and experiment-to-experiment variations, hind limb blood flow was expressed as the ratio of left (ischemic) to right (non-ischemic) laser-Doppler signal.

Micro-CT angiography. Micro-CT angiography and analysis were carried out as described (30).

Briefly, 2D micro-CT images were acquired with a GE eXplore Locus SP scanner (GE Healthcare), using 360 views with angular increment of 0.5 degree and 24-μm isotropic resolution at a voltage of 60 kVp and 100 mAs tube current. Micro-CT data were transferred via Microview software (version 2.2; GE Healthcare) to the Advanced Workstation (version 4.4; GE Healthcare) for vascular segmentation. National Institutes of Health ImageJ was used to analyze vascular tree. Data are expressed as a vascular segment number, representing the total number of vessels of specified diameter counted in 200 *z* sections for calf in 3D micro-CT images.

Statistical Analysis. Statistical analysis was performed by using GraphPad Prism software v.5. Photoshop CS5 software was used for image processing in compliance with general guidelines for image processing. All data are presented as mean ± SD, and two group comparisons were done with a two-tailed Student *t* test. A value of $P < 0.05$ was taken as statistically significant.

ACKNOWLEDGMENTS. We thank Robert Friesel (Maine Medical Center Research Institute) for providing *Frs2α* and VEGFR2 constructs; Ralf Adams (Max Planck Institute, Munster) for *Cdh5-CreERT2* mouse; Marcus Fruttiger (University College London) for PDGF-BB-CreERT2 mouse; Fen Wang (Texas A&M Health Science Center) for *Frs2α*$^{fl/fl}$ mice; Veraragavan P. Eswarakumar (Yale University) for *Frs2α*$^{4F/4F}$ mice; and Rita Webber, Nicole Copeland, and Wayne Evangelisti for maintaining the mice used in these studies. This work was supported by National Institutes of Health Grants R01 HL084619 (to M.S.).

1. Carmeliet P, Jain RK (2011) Molecular mechanisms and clinical applications of angiogenesis. *Nature* 473(7347):298–307.
2. Lohela M, Bry M, Tammela T, Alitalo K (2009) VEGFs and receptors involved in angiogenesis versus lymphangiogenesis. *Curr Opin Cell Biol* 21(2):154–165.
3. Benedito R, et al. (2012) Notch-dependent VEGFR3 upregulation allows angiogenesis without VEGF-VEGFR2 signalling. *Nature* 484(7392):110–114.
4. Wang Y, et al. (2010) Ephrin-B2 controls VEGF-induced angiogenesis and lymphangiogenesis. *Nature* 465(7297):483–486.
5. Sawamiphak S, et al. (2010) Ephrin-B2 regulates VEGFR2 function in developmental and tumour angiogenesis. *Nature* 465(7297):487–491.
6. Lee S, et al. (2007) Autocrine VEGF signaling is required for vascular homeostasis. *Cell* 130(4):691–703.
7. Koch S, Tugues S, Li X, Gualandi L, Claesson-Welsh L (2011) Signal transduction by vascular endothelial growth factor receptors. *Biochem J* 437(2):169–183.
8. Kouhara H, et al. (1997) A lipid-anchored Grb2-binding protein that links FGF-receptor activation to the Ras/MAPK signaling pathway. *Cell* 89(5):693–702.
9. Gotoh N, Laks S, Nakashima M, Lax I, Schlessinger J (2004) FRS2 family docking proteins with overlapping roles in activation of MAP kinase have distinct spatial-temporal patterns of expression of their transcripts. *FEBS Lett* 564(1-2):14–18.
10. Ong SH, et al. (2000) FRS2 proteins recruit intracellular signaling pathways by binding to diverse targets on fibroblast growth factor and nerve growth factor receptors. *Mol Cell Biol* 20(3):979–989.
11. Sato T, Gotoh N (2009) The FRS2 family of docking/scaffolding adaptor proteins as therapeutic targets of cancer treatment. *Expert Opin Ther Targets* 13(6):689–700.
12. Gotoh N (2008) Regulation of growth factor signaling by FRS2 family docking/scaffold adaptor proteins. *Cancer Sci* 99(7):1319–1325.
13. Hama J, Xu H, Goldfarb M, Weinstein DC (2001) SNT-1/FRS2alpha physically interacts with Laloo and mediates mesoderm induction by fibroblast growth factor. *Mech Dev* 109(2):195–204.
14. Gotoh N, et al. (2004) Tyrosine phosphorylation sites on FRS2alpha responsible for Shp2 recruitment are critical for induction of lens and retina. *Proc Natl Acad Sci USA* 101(49):17144–17149.
15. Kameda Y, Ito M, Nishimaki T, Gotoh N (2008) FRS2 alpha 2F/2F mice lack carotid body and exhibit abnormalities of the superior cervical sympathetic ganglion and carotid sinus nerve. *Dev Biol* 314(1):236–247.
16. Lanahan AA, et al. (2010) VEGF receptor 2 endocytic trafficking regulates arterial morphogenesis. *Dev Cell* 18(5):713–724.
17. Drappa J, et al. (2003) Impaired T cell death and lupus-like autoimmunity in T cell-specific adapter protein-deficient mice. *J Exp Med* 198(5):809–821.
18. Sun Z, et al. (2012) VEGFR2 induces c-Src signaling and vascular permeability in vivo via the adaptor protein TSAd. *J Exp Med* 209(7):1363–1377.
19. Sakurai Y, Ohgimoto K, Kataoka Y, Yoshida N, Shibuya M (2005) Essential role of Flk-1 (VEGF receptor 2) tyrosine residue 1173 in vasculogenesis in mice. *Proc Natl Acad Sci USA* 102(4):1076–1081.
20. Zhou W, et al. (2009) FGF-receptor substrate 2 functions as a molecular sensor integrating external regulatory signals into the FGF pathway. *Cell Res* 19(10):1165–1177.
21. Hadari YR, Gotoh N, Kouhara H, Lax I, Schlessinger J (2001) Critical role for the docking-protein FRS2 alpha in FGF receptor-mediated signal transduction pathways. *Proc Natl Acad Sci USA* 98(15):8578–8583.
22. Lanahan A, et al. (2013) The neuropilin 1 cytoplasmic domain is required for VEGF-A-dependent arteriogenesis. *Dev Cell* 25(2):156–168.
23. Stoletov KV, Ratcliffe KE, Terman BI (2002) Fibroblast growth factor receptor substrate 2 participates in vascular endothelial growth factor-induced signaling. *FASEB J* 16(10):1283–1285.
24. Hatanaka K, Simons M, Murakami M (2011) Phosphorylation of VE-cadherin controls endothelial phenotypes via p120-catenin coupling and Rac1 activation. *Am J Physiol Heart Circ Physiol* 300(1):H162–H172.
25. Chen PY, et al. (2012) FGF regulates TGF-β signaling and endothelial-to-mesenchymal transition via control of let-7 miRNA expression. *Cell Rep* 2(6):1684–1696.
26. Eswarakumar VP, Horowitz MC, Locklin R, Morriss-Kay GM, Lonai P (2004) A gain-of-function mutation of Fgfr2c demonstrates the roles of this receptor variant in osteogenesis. *Proc Natl Acad Sci USA* 101(34):12555–12560.
27. Lin Y, Zhang J, Zhang Y, Wang F (2007) Generation of an Frs2alpha conditional null allele. *Genesis* 45(9):554–559.
28. Pitulescu ME, Schmidt I, Benedito R, Adams RH (2010) Inducible gene targeting in the neonatal vasculature and analysis of retinal angiogenesis in mice. *Nat Protoc* 5(9):1518–1534.
29. Claxton S, et al. (2008) Efficient, inducible Cre-recombinase activation in vascular endothelium. *Genesis* 46(2):74–80.
30. Murakami M, et al. (2011) FGF-dependent regulation of VEGF receptor 2 expression in mice. *J Clin Invest* 121(7):2668–2678.